J. Fluid Mech. (2010), *vol.* 647, *pp.* 403–419.
doi:10.1017/S002211200999320X

Monolayer slip effects on the dynamics of a lipid bilayer vesicle in a viscous flow

JONATHAN T. SCHWALBE[1], PETIA M. VLAHOVSKA[2] AND MICHAEL J. MIKSIS[1]†

[1]Department of Engineering Sciences and Applied Mathematics, Northwestern University, Evanston, IL 60202, USA

[2]Thayer School of Engineering, Dartmouth College, Hanover, NH 03755, USA

(Received 13 August 2009; revised 29 October 2009; accepted 29 October 2009)

The dynamics of a closed lipid bilayer membrane (a vesicle) in a linear viscous flow is investigated. The model accounts for the transport of lipids along each monolayer and intermonolayer friction, as well as the membrane fluidity, incompressibility and resistance to bending. Assuming a nearly spherical vesicle, the leading order analysis results in a nonlinear coupled system of equations for the dynamics of the shape and the bilayer density difference. Multiple solution states are found as a function of viscosity ratio and the monolayer slip coefficient. The dynamics and stability of these solutions is discussed.

1. Introduction

Phospholipid bilayer membranes are a key component of biological cells (Alberts 2002). Vesicles, which are bags made of such bilayers, play a vital role in physiological processes such as synaptic transmission and intracellular trafficking. Vesicles also find biomedical applications as vectors for drug and gene delivery (Allen & Cullis 2004). In vitro produced vesicles mimic a variety of cellular phenomena and hence vesicles are widely employed as a simple cell model (Abkarian & Viallat 2008). For example, a giant vesicle exhibits the essential characteristics of the red blood cell such as its equilibrium biconcave shape (Seifert 1997), and its non-equilibrium behaviour, e.g. tumbling under flow (Kantsler & Steinberg 2006).

The physical properties of lipid bilayers and equilibrium vesicle configurations have been extensively studied (Seifert 1997). Lipid molecules self-assemble into membranes, which consist of two lipid monolayers. Lipid bilayers spontaneously close to avoid exposure of their hydrophobic core to water, and form vesicles. Vesicle conformations are governed by curvature energy (Lipowsky 1991), unlike drops whose shape is controlled by surface tension and capsules, whose polymerized membranes are solid elastic (Barthes-Biesel & Rallison 1981; Barthes-Biesel 1991; Pozrikidis 2003). The simplest physical model proposed by Helfrich (1973) treats the bilayer as a two-dimensional surface and the total bending energy of a vesicle is

$$\mathscr{F} = \frac{\kappa}{2}\int (2H)^2 \mathrm{d}A, \tag{1.1}$$

† Email address for correspondence: miksis@northwestern.edu

where κ is the bending modulus and H is the mean curvature. Phospholipid membranes are remarkably soft, because the energy required for bending is comparable to the thermal energy; bending rigidity is $\kappa \sim 20 k_B T$ (Dimova *et al.* 2006). At physiological temperatures, lipid molecules are free to move within the monolayer, and therefore, in contrast to solid-like polymerized membranes, the lipid bilayer membrane is fluid with a zero shear-elastic modulus. Owing to its simplicity, the minimal model given by (1.1) has been widely employed in studies of equilibrium vesicle dynamics, i.e. membrane fluctuations around locally stable shape (Milner & Safran 1987; Brown 2008), as well as non-equilibrium dynamics such as vesicles in flow (Seifert 1999; Misbah 2006; Danker, Vlahovska & Misbah 2009). These works account for the fixed number of lipids in the membrane by enforcing that the interface is area incompressible. Accordingly, a tension field is introduced, which has to be determined self-consistently with deformation. The leading-order analysis for a nearly spherical vesicle in shear flow has shown that the dynamics is nonlinear due to the shape-dependant tension (Seifert 1999; Olla 2000; Misbah 2006; Vlahovska & Gracia 2007). The shape evolution is described by a set of coupled quadratic equations which predict tank treading, where the vesicle deforms into a prolate ellipsoid inclined at a stationary angle close to $\pi/4$ with respect to the flow direction, or tumbling dynamics, where the vesicle undergoes a periodic flipping motion. The theory agrees well with experiments (Kantsler & Steinberg 2005, 2006; Mader *et al.* 2006; Deschamps, Kantsler & Steinberg 2009), reviewed in Abkarian & Viallat (2008). Interestingly, according to the leading-order theory, the tank treading to tumbling transition is controlled by the viscosity ratio and it is independent of the shear rate. The effect of shear rate enters at next order (Danker *et al.* 2007; Lebedev, Turitsyn & Vergeles 2008).

The minimal model captures the vesicle physics only to a limited extent because it neglects the bilayer architecture of the membrane. For example, the predicted phase diagram of equilibrium shapes is incomplete (Seifert 1997). A more realistic approach for planar membranes, which we employ here, treats the membrane as being composed of two slightly coupled monolayers and was proposed by Seifert & Langer (1993). Their formulation is at the heart of the area-difference-elasticity model, which has successfully explained the variety of static vesicle shapes (Seifert, Berndl & Lipowsky 1991; Dobereiner *et al.* 1997). Bending the bilayer membrane leads to compression and stretching of the monolayers. The resulting density inhomogeneities relax by lipid flow within the monolayers; note that lipids can not transport between the monolayers due to the high energy cost for such 'flip–flop'. In addition, the weak non-covalent bonds between the two monolayers allow the two monolayers to slide over each other (Evans *et al.* 1992). The lipid redistribution and intermonolayer friction modify the membrane dynamics and give rise to a new mode in the equilibrium fluctuations of a planar lipid membrane, in addition to the bending mode predicted by the minimal model (Seifert & Langer 1993). Non-planar shapes have also been analysed, such as a sphere (Miao, Lomholt & Kleis 2002) and a tube (Goldstein *et al.* 1996). However, the effects of lipid dynamics on the overall vesicle non-equilibrium behaviour have not been addressed so far.

The goal of this paper is to develop a theory for the vesicle dynamics which uses the more natural language of lipid density fields instead of tension. Thus, effects of lipid density variations and bilayer slip can be explored. We generalize work by Miao *et al.* (2002) on equilibrium dynamics of a quasi-spherical vesicle to include a viscosity contrast and an imposed linear flow. The lipid conservation is enforced and the constraint on total lipid number is compared to the area constraint used by the approaches based on the minimal model.

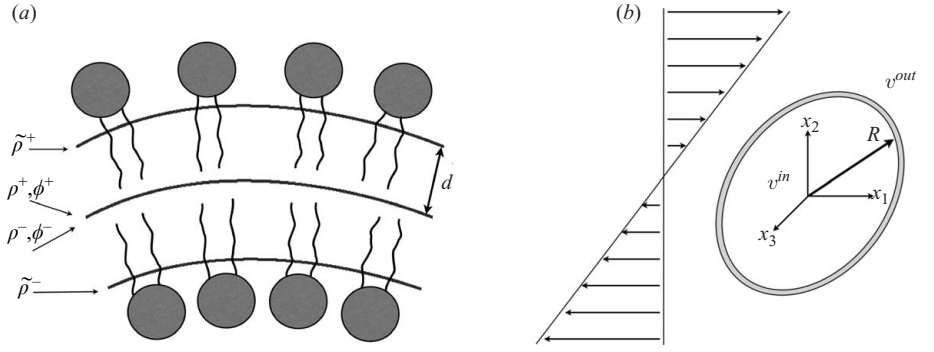

FIGURE 1. (*a*) Structure of a lipid membrane formed by two identical monolayers. At the monolayer's neutral surface, bending and stretching are decoupled. For a symmetric bilayer, the monolayers neutral surfaces are distance $2d$ apart. (*b*) Sketch of a vesicle in a simple shear flow.

2. Problem formulation

Let us consider a neutrally buoyant vesicle suspended in a fluid of viscosity μ^{out} and filled with a fluid of viscosity μ^{in}. Both interior and exterior fluids are incompressible and Newtonian. The vesicle is placed in a simple shear flow, which in a Cartesian coordinate system centred in the vesicle is given by $\boldsymbol{v}^{\infty}(\mathbf{r}) = \dot{\gamma}\boldsymbol{E}\cdot\boldsymbol{r}$. The velocity gradient tensor is $E_{ij} = \delta_i^1\delta_j^2$ and the strain rate $\dot{\gamma}$ is assumed to be constant; δ_i^j is the Kronecker delta function. A sketch of the problem is shown in figure 1(*b*).

Our aim is to obtain the flow about the vesicle and the evolution of the vesicle shape. At the length scale of a micron-size vesicle low-Reynolds-number (creeping flow) conditions prevail. Accordingly, fluid motion is described by the Stokes equations,

$$\mu^{(a)}\nabla^2\boldsymbol{v}^{(a)} - \nabla p^{(a)} = 0, \quad \nabla\cdot\boldsymbol{v}^{(a)} = 0; \quad (a) = in,\ out, \tag{2.1}$$

where $p^{(a)}$ is the pressure and $\boldsymbol{v}^{(a)}$ denotes the fluid velocity. Note that superscripts are used to distinguish variables inside and outside the vesicle. Far away from the vesicle, the flow tends to the unperturbed external flow $\boldsymbol{v}^{out} \to \boldsymbol{v}^{\infty}$. The boundary conditions are nontrivial, as the interior and suspending fluids are separated by a bilayer membrane composed of two monolayers (see figure 1(*a*)). The outer monolayer, which faces the suspending fluid, contains N^+ lipids, while the inner monolayer contains N^- lipids. The local surface number density of lipids defined on a monolayer's neutral surface is $\tilde{\rho}^{\pm}$. The focus of our study is on giant vesicles ($\sim 10\,\mu$m or larger), and therefore the molecularly thin membrane can be approximated as a two-dimensional surface embedded in three-dimensional space. The vesicle boundary is defined by the bilayer midplane, which is located at a half-distance d between the monolayer neutral surfaces. The vesicle shape is then specified by the position of the bilayer midplane $\boldsymbol{R}(u^1, u^2, t)$, where (u^1, u^2) are surface coordinates. The vesicle's characteristic size is defined by the radius of a sphere of the same volume R_0. The membrane is impermeable and hence the velocity normal to the membrane is continuous. However intermonolayer friction gives rise to a tangential slip. Across the boundary, the hydrodynamic stresses undergo a jump, which is balanced by membrane surface forces. In the remainder of this section we discuss the membrane tractions and the evolution equations of shape and lipid distribution.

2.1. *Thermodynamic free energy of a bilayer membrane*

Here we summarize the model formulated by Seifert & Langer (1993). The free energy density on the bilayer midplane surface is

$$\frac{\mathrm{d}\mathscr{F}}{\mathrm{d}A} = \frac{\kappa}{2}(2H)^2 + \frac{K_A}{2}\left[(\phi^+ - 2dH)^2 + (\phi^- + 2dH)^2\right] + \sigma\,, \tag{2.2}$$

where κ is the bilayer bending rigidity, K_A is the monolayer compressibility modulus, H is the mean curvature and σ is the membrane tension. Contributions that integrate to constants are neglected. The monolayer lipid densities are projected onto the bilayer midplane using the parallel surfaces approximation. At leading order in dH, $\tilde{\rho}^{\pm} = \rho^{\pm}(1 \mp dH)$. It is convenient to introduce $\phi^{\pm}$ as $\rho^{\pm} = \rho_0(1 + \phi^{\pm})$ with $\rho_0 = (\rho^+ + \rho^-)/2$, where at equilibrium $\rho^{\pm} = \rho_0^{\pm} = N^{\pm}/A_0$ and corresponds to the area per lipid at equilibrium, in the absence of flow. Here A_0 is the area of the surface defined by the bilayer midplane.

The first term in (2.2) reflects the energy cost for bending of the bilayer. The second term describes the free energy cost for creating inhomogeneous lipid distribution, in other words the elastic energy density of each monolayer. The last term is the free energy cost of changing the area of the vesicle at a constant lipid density with σ acting as the effective membrane tension (Miao *et al.* 2002). The need for variable σ will be highlighted in § 3.1. Rearranging the terms in (2.2) yields

$$\mathscr{F} = \int \mathrm{d}A\frac{\kappa_{eff}}{2}(2H)^2 + \int \mathrm{d}A\frac{K_A}{2}\left[(\phi^+)^2 + (\phi^-)^2\right] + \int \mathrm{d}A\lambda H(\phi^+ - \phi^-) + \int \mathrm{d}A\sigma. \tag{2.3}$$

The parameter $\kappa_{eff} = \kappa + 2d^2K_A$ is a renormalized bilayer bending rigidity. The elastic terms have been expanded and grouped to give the third term which describes the free energy cost associated with any coupling between changes in curvature and local lipid densities, where $\lambda = 2dK_A$ (Seifert & Langer 1993; Miao *et al.* 2002).

2.2. *Interfacial mechanics of a bilayer membrane*

Here we outline the transport equations of lipid mass and momentum on the bilayer midplane. Detailed discussion can be found in Edwards, Brenner & Wasan (1991), Aris (1989), Stone (1990) and Cai & Lubensky (1995). Each lipid monolayer is treated as a two-dimensional fluid with velocity $\boldsymbol{v}^{\pm}$. Since there is no exchange of lipids between the monolayers, the total number of lipids in a monolayer is conserved

$$\frac{\partial \rho^{\pm}}{\partial t} + \nabla_s \cdot (\rho^{\pm}\boldsymbol{v}_s^{\pm}) + \rho^{\pm}(\nabla_s \cdot \boldsymbol{n})(\boldsymbol{v}^{\pm} \cdot \boldsymbol{n}) = 0, \tag{2.4}$$

where $\boldsymbol{v}^{\pm}$ is the fluid velocity at each interface, $\boldsymbol{v}_s^{\pm} = (\boldsymbol{I} - \boldsymbol{nn}) \cdot \boldsymbol{v}^{\pm}$ is the velocity component tangential to the surface, and ∇_s is the surface gradient operator defined as, $\nabla_s = (\boldsymbol{I} - \boldsymbol{nn}) \cdot \nabla$, where $\boldsymbol{n}$ is the local unit normal vector and $\boldsymbol{I}$ is the identity matrix. Note that $\boldsymbol{v}^{\pm} \cdot \boldsymbol{n}$ is continuous across the surface. Our concern is membrane fluctuations with wavelengths comparable to that of the size of the vesicle, therefore intrinsic dissipation within the monolayers is negligible and any diffusion flux can be neglected (Yeung & Evans 1995).

The lipid membrane stores elastic energy in bending as well as compression or stretching of the lipid monolayers. Dissipation is mainly due to two sources: bulk fluid viscosity and intermonolayer friction. The momentum conservation reflects the balance of dissipative and restoring forces. In the overdamped limit, it reduces to

$$\boldsymbol{t}_{hd}^{\pm} + \boldsymbol{t}_{m}^{\pm} + \boldsymbol{t}_{rs}^{\pm} = 0\,, \tag{2.5}$$

where $\boldsymbol{t}_{hd}^{\pm}$ are the tractions exerted on the monolayer surfaces by the bulk fluids, $\boldsymbol{t}_{rs}^{\pm}$ are mechanical restoring forces associated with the free energy of the system (2.3) and $\boldsymbol{t}_{m}^{\pm}$ are surface forces associated with dissipation in the membrane.

These three contributions will now be discussed in detail.

2.2.1. *Membrane restoring (elastic) forces*

The general form of the mechanical restoring forces $\boldsymbol{t}_{rs}$ for a vesicle of an arbitrary shape has been obtained by taking a variation of the free energy $\delta\mathscr{F}$ (Jenkins 1977; Cai & Lubensky 1995; Miao *et al.* 2002):

$$\boldsymbol{t}_{rs}^{\pm} = \Bigg[-\kappa_{eff}\left[H(2H^2-2K)+\Delta H\right] - \pi^{\pm}(2H) \mp \lambda \times \left(\frac{1}{2}\Delta\phi^{\pm} + (2H^2-K)\phi^{\pm} + 2H^2\right)\Bigg]\boldsymbol{n} - \nabla_s\pi^{\pm} \mp \lambda(1+\phi^{\pm})\nabla_s H, \tag{2.6}$$

where Δ is the Laplace–Beltrami operator. Both curvatures, mean, $H=(c_1+c_2)/2$, and Gaussian, $K=c_1c_2$, appear as well as the new parameter $\pi^{\pm}=-\sigma/2+K_A\phi^{\pm}+\frac{K_A}{2}(\phi^{\pm})^2$ which can be thought of as the monolayer surface pressures. The quantities c_1 and c_2 are the two principal curvatures.

2.2.2. *Dissipative forces*

The membrane viscosity of fluid lipid bilayers is relatively low, $\sim 10^{-9}$ Ns m^{-1} (Dimova *et al.* 2006), and its effects are usually negligible. Moreover, as discussed in Yeung & Evans (1995) the drag between the monolayers scales as the inverse of the membrane thickness and thus dominates over the surface viscous effects, which scale with the membrane thickness. Therefore, effects of surface viscosity were neglected in this study.

The intermonolayer friction is described by the following phenomenological relation (Evans *et al.* 1992):

$$\boldsymbol{t}_{m}^{\pm} = \mp b(\boldsymbol{v}_s^{+} - \boldsymbol{v}_s^{-}), \tag{2.7}$$

where the parameter b is the slip coefficient. Its magnitude varies greatly depending on the type of lipid; values of b have been reported from 10^4 to 10^9 Ns m^{-4} (Merkel, Sackmann & Evans 1989; den Otter & Shkulipa 2007).

The bulk hydrodynamic stress is given by $\boldsymbol{T}^{(a)} = -p^{(a)}\mathbf{I} + \mu^{(a)}\left[\nabla\boldsymbol{v}^{(a)} + (\nabla\boldsymbol{v}^{(a)})^{\dagger}\right]$, where $\dagger$ denotes the transpose. The hydrodynamic forces per unit area on each monolayer are then $\boldsymbol{t}_{hd}^{+} = \boldsymbol{T}^{out}|_{\boldsymbol{r}=\boldsymbol{R}}\cdot\boldsymbol{n}$ and $\boldsymbol{t}_{hd}^{-} = -\boldsymbol{T}^{in}|_{\boldsymbol{r}=\boldsymbol{R}}\cdot\boldsymbol{n}$.

2.3. *Solution outline*

In summary, the Stokes' equations (2.1) are solved in the interior and exterior of the vesicle subject to the far field condition imposed by the external flow. The surface velocity of the interface matches the velocity of the adjacent bulk fluid. The stress conditions, (2.5), plus the transport equation of lipid density, (2.4), are applied on each monolayer. Together these equations determine the dynamics of the interface and the lipid density fields on each monolayer.

3. Solution for a nearly spherical vesicle

In this study, we focus on a vesicle with a shape close to a sphere. We non-dimensionalize all variables using $\dot{\gamma}^{-1}$ as the characteristic time scale and the effective equilibrium radius R_0 as a length scale. Accordingly, stresses are rescaled by $\mu^{out}\dot{\gamma}$

and velocity by $R_0\dot{\gamma}$. The non-dimensionsionalization gives rise to the following dimensionless parameters,

$$Ca = \frac{\mu^{out} R_0^3 \dot{\gamma}}{\kappa_{eff}}, \quad \beta = \frac{b R_0^4 \dot{\gamma}}{\kappa_{eff}}, \quad \eta = \frac{\mu^{in}}{\mu^{out}}, \quad \alpha = \frac{K_A R_0^2}{\kappa_{eff}}, \quad \Lambda = \frac{\lambda R_0}{\kappa_{eff}}. \tag{3.1}$$

The capillary number Ca characterizes the strength of the imposed flow. The parameter β is the dimensionless friction (slip) coefficient where large β implies large friction between the monolayers, while small β corresponds to two freely slipping monolayers. The rest of the parameters are flow–independent and related to the physical properties of the system. For example, the dimensionless compressibility α measures the monolayer's ability to change local area; small α describes a compressible monolayer.

Due to the symmetry, the spherical coordinate system (θ, ϕ, r), with basis vectors, $\boldsymbol{e}_\theta$, $\boldsymbol{e}_\phi$ and $\boldsymbol{e}_r$, is the natural choice to describe the system. The three-dimensional vector which represents the surface of the vesicle is written as

$$\boldsymbol{R}(u^1, u^2, t) = \boldsymbol{R}(\theta, \phi, t) = R(\theta, \phi, t)\boldsymbol{e}_r = [1 + f(\theta, \phi, t)]\boldsymbol{e}_r, \tag{3.2}$$

where $f(\theta, \phi, t)$ is a small perturbation from the spherical reference shape and $f \sim \epsilon \ll 1$. The small parameter ϵ measures the deviations from sphericity. We will assume that all velocities, shape variables f and density fields $\phi^{\pm}$ are order ϵ terms. Owing to the spherical symmetry, all perturbation fields are expanded in the basis of spherical harmonics, $\mathscr{Y}_{lm}$ (Morse & Feshbach 1953),

$$f(\theta, \phi, t) = \epsilon \sum_{l,m} f_{lm}(t)\mathscr{Y}_{lm}(\theta, \phi), \tag{3.3}$$

$$\phi^{\Delta}(\theta, \phi, t) = \epsilon \left[\phi_0^{\Delta} + \left(\sum_{l,m} \psi_{lm}^{\Delta}(t)\mathscr{Y}_{lm}(\theta, \phi) + \frac{1}{\sqrt{4\pi}} \psi_{00}^{\Delta} \right) \right], \tag{3.4}$$

$$\phi^{\Sigma}(\theta, \phi, t) = \epsilon \left(\sum_{l,m} \psi_{lm}^{\Sigma}(t)\mathscr{Y}_{lm}(\theta, \phi) + \frac{1}{\sqrt{4\pi}} \psi_{00}^{\Sigma} \right), \tag{3.5}$$

where l takes values from 2 to ∞ and m between $-l$ and l. The $l = 1$ modes are omitted because they describe translation of the centre of mass. We have introduced the mean density perturbation, $\phi^{\Sigma} = (\phi^{+} + \phi^{-})/2$, and the density difference, $\phi^{\Delta} = (\phi^{+} - \phi^{-})/2$. The quantity ϕ_0^{Δ} characterizes the equilibrium density difference distribution on the vesicle. Typically, $\phi_0^{\Delta} \neq 0$ as the vesicle formation process leads to different number of lipids in the monolayers, i.e. $N^{+} \neq N^{-}$. The global conservation of lipids on the surface, $\int (1 + \phi^{\pm}) dA = \rho_0^{-1} N^{\pm}$, shows that $\psi_{00}^{\Delta/\Sigma}$ are $O(\epsilon)$; this relation serves to fix $\psi_{00}^{\Delta/\Sigma}$ in terms of lower order terms in ϵ.

The Stokes' equations for flow past a vesicle are solved using the Lamb solution. All quantities are expanded to first order in ϵ. The stress balance equations (A 1), (A 2) and (A 3) are evaluated on a sphere. The kinematic condition and lipid conservation yield the evolution equations for f_{lm}, ψ_{lm}^{Δ} and ψ_{lm}^{Σ}. Details of the solution are given in the Appendices A and B.

3.1. *Conservation of lipids: elimination of the ψ_{lm}^{Σ} mode*

The total number of lipids in each monolayer is constant. Examination of the three characteristic membrane time scales in this problem corresponding to bending (t_c),

intermonolayer friction (t_b) and monolayer compression (t_{K_A}) shows that

$$t_c = \frac{\mu^{out} R_0^3}{\kappa_{eff}} \sim 10s\,, \quad t_b = \frac{bR_0^2}{K_A} \sim 1.6s\,, \quad t_{K_A} = \frac{\mu^{out} R_0}{K_A} \sim 3 \times 10^{-7} s\,, \tag{3.6}$$

where $\mu^{out} = 0.001$ N s m^{-2}, $R_0 = 10^{-5}$ m, $\kappa_{eff} = 10^{-19}$ J, $K_A = 0.03$ J m^{-2} and $b = 5 \times 10^8$ J s m^{-4} (Seifert & Langer 1993). This large separation of time scales allows us to set (Goldstein *et al.* 1996; Miao *et al.* 2002)

$$\frac{\mathrm{d}\psi_{lm}^{\Sigma}}{\mathrm{d}t} = 0\,. \tag{3.7}$$

This condition is analogous to the 'local area incompressibility' constraint used in previous work (Schneider, Jenkins & Webb 1984; Milner & Safran 1987; Seifert 1999; Vlahovska & Gracia 2007). It means that local changes in the average of the projected densities relax faster than changes in shape or local density difference (Goldstein *et al.* 1996). As pointed out in Miao *et al.* (2002) this constraint is not to be directly compared to incompressibility of the bulk fluids because only one mode of monolayer density relaxation ψ_{lm}^{Σ} can be eliminated by invoking it (ψ_{lm}^{Δ} remains). This added constraint will be treated as an extra equation in the system which will have to be explicitly enforced. In order to incorporate the constraint (3.7), we introduce an unknown variable membrane tension in the formulation of the problem (see (2.3)),

$$\sigma(\theta, \phi, t) = \sigma_0 + \sum_{l,m} \sigma_{lm}(t) \mathscr{Y}_{lm}(\theta, \phi). \tag{3.8}$$

The global expression for constraint total number of lipids on each monolayer surface leads to,

$$\frac{\mathrm{d}}{\mathrm{d}t} \int_{\Omega} (1 + \phi^{\pm}) \frac{R^2}{\boldsymbol{e_r} \cdot \mathbf{n}} \mathrm{d}\Omega = 0, \tag{3.9}$$

where $R^2/\boldsymbol{e_r} \cdot \mathbf{n}$ is the Jacobian of the transformation from the nearly spherical shape, to the spherical shape defined by the sold angle Ω. Following a similar set of manipulations to that of Vlahovska & Gracia (2007) the integration over the solid angel becomes at leading order in ϵ,

$$\frac{\mathrm{d}}{\mathrm{d}t} \left[\sum_{l,m} \tilde{a}(l) f_{lm} f_{lm}^{*} + 2 \sum_{l,m} f_{lm} \psi_{lm}^{*\pm} + 4\pi \psi_{00}^{\pm} \right] = 0 \tag{3.10}$$

with $\tilde{a}(l) = (l+2)(l-1)/2$, and $\psi_{lm}^{\pm}$ are the amplitudes of modes in the spherical harmonics expansion for the lipid density fields $\phi^{\pm}$. Note that $\psi_{lm}^{\Delta/\Sigma} = (\psi_{lm}^{+} \mp \psi_{lm}^{-})/2$. Taking the average of the two equations above (one corresponding to the outer monolayer '+' and the other to the inner monolayer '−'), using the fact that $\dot{\psi}_{lm}^{\Sigma} = 0$ for all l and m and assuming an initial condition of $\psi_{lm}^{\Sigma}(0) = 0$ we arrive at

$$\sum_{l,m} \tilde{a}(l) \dot{f}_{lm} f_{lm}^{*} = 0\,, \tag{3.11}$$

where the superscript $*$ denotes complex conjugate and dot is a time derivative. Analogous relation was derived in the minimal model theories from the area constraint (Milner & Safran 1987; Vlahovska & Gracia 2007).

Taking the difference of the '+' and the '−' equations in (3.10) leads to an expression, from which ψ_{00}^{Δ} can be determined in terms of f_{lm} and ψ_{lm}^{Δ}.

3.2. *Evolution equations in a general flow*

Detailed in the Appendices are the calculations leading to the shape and density evolution equations. The nonuniform component of the tension is eliminated from the problem by use of tangential stress balance (A 2). The field ψ^{Σ}_{lm} is determined up to a constant by (3.7) leaving the following two equations of motion for the remaining two unknown perturbation fields, $f_{lm}(t)$ and $\psi^{\Delta}_{lm}(t)$,

$$\Gamma(\eta,l)\frac{\mathrm{d}f_{lm}}{\mathrm{d}t}+J(\eta,l)\frac{\mathrm{d}\psi^{\Delta}_{lm}}{\mathrm{d}t}=Ca^{-1}\big[l(l+1)\tilde{E}_l f_{lm} + l(l+1)a(l)\sigma_0 f_{lm}-D(l)\psi^{\Delta}_{lm}\big]+C(l,m) \quad (3.12)$$

and

$$\hat{\Gamma}(\eta,l)\frac{\mathrm{d}f_{lm}}{\mathrm{d}t}+\hat{J}(\eta,l)\frac{\mathrm{d}\psi^{\Delta}_{lm}}{\mathrm{d}t}=Ca^{-1}\Big[D(l)f_{lm}-2\alpha l(l+1)\psi^{\Delta}_{lm} - 2\phi^{\Delta}_0\alpha l(l+1)\psi^{\Sigma}_{lm}\Big]+\hat{C}(l,m). \quad (3.13)$$

Explicit expressions for coefficients are listed in Appendix C. Present in the first of the above two equations of motion is the quantity σ_0, the isotropic component of the membrane tension. It depends on the instantaneous shape and lipid distribution (see (C 9)), and thus makes this system nonlinear to leading order as opposed to capsules and drops (Barthes-Biesel & Rallison 1981; Barthes-Biesel 1991; Pozrikidis 2003). The coefficients, which are dependent on the viscosity contrast, yield combinations which are bounded as $\eta\to\infty$. The last term in each of the above equations describes the distortion of the vesicle by the imposed flow. All terms multiplied by Ca^{-1} represent relaxation driven by membrane elastic stresses.

3.3. *Simple shear flow*

Simple shear flow can be decomposed into rotation and extension. The extensional part of the flow deforms the vesicle; its action is described by the inhomogeneous terms in (3.12) and (3.13)

$$C(2,\pm2)=\delta_l^2\delta_m^{\pm2}\left(\pm\frac{84\mathrm{i}}{15}\sqrt{30\pi}\right) \quad (3.14)$$

and

$$\hat{C}(2,\pm2)=\delta_l^2\delta_m^{\pm2}\left(\pm\frac{12\mathrm{i}}{5}\sqrt{30\pi}\right). \quad (3.15)$$

Therefore, only $l=2$ (ellipsodial) shape and density modes are excited at leading order (Vlahovska & Gracia 2007) (see Appendix A.2). Since the vesicle shape is initially non-spherical, the rotational flow component affects the leading order evolution equations. The kinematic condition is $\dot{R}=\boldsymbol{v}\cdot\hat{\boldsymbol{e}}_r-\boldsymbol{v}\cdot\nabla R$. The extensional component of the applied flow is exactly balanced by the extensional component of the flow perturbation due to the vesicle because the surface flow is area incompressible at leading order (Seifert 1999). Hence,

$$\boldsymbol{v}^{\infty}_{rot}\cdot\nabla R=-\mathrm{i}\omega\frac{m}{2}f_{lm}. \quad (3.16)$$

This can also be interpreted as a rotation of the coordinate system where ω is the magnitude of the rotational component of the flow field. For simple shear flow $\omega=1$. This term is combined with the regular time derivative to form the Jaumann

derivative, $\mathrm{d}/\mathrm{d}t = \partial/\partial t - \mathrm{i}\omega(m/2)$, which at this order fully accounts for the rotational component of the flow (see e.g. Danker *et al.* 2007).

Finally, the evolution equations in shear flow take the form,

$$\begin{aligned}\Gamma(\eta,2)\dot{f}_{2m} + J(\eta,2)\dot{\psi}^{\Delta}_{2m} = {} & \frac{\mathrm{i}m}{2}\left[\Gamma(\eta,2)f_{2m} + J(\eta,2)\psi^{\Delta}_{2m}\right] + C(2,m) + 2\Delta^{-1} \\ & \times \left(C(2,2) - \mathscr{J}\hat{C}(2,2)\right)(f_{22} - f_{2-2})f_{2m} + 24^{-1} \\ & \times \left(\mathscr{J}(\eta,2)f_{2m} - \psi^{\Delta}_{2m}\right) + 24Ca^{-1}\Delta^{-1}(2\Lambda - \alpha\mathscr{J}) \\ & \times \left(\psi^{\Delta}_{2-2}f_{22} + \psi^{\Delta}_{20}f_{20} + \psi^{\Delta}_{22}f_{2-2}\right) f_{2m} \end{aligned} \tag{3.17}$$

and

$$\begin{aligned}\hat{\Gamma}(\eta,2)\dot{f}_{2m} + \hat{J}(\eta,2)\dot{\psi}^{\Delta}_{2m} = {} & \frac{\mathrm{i}m}{2}\left[\hat{\Gamma}(\eta,2)f_{2m} + \hat{J}(\eta,2)\psi^{\Delta}_{2m}\right] + \hat{C}(2,m) \\ & + 12Ca^{-1}\left[2\Lambda f_{2m} - \alpha\left(\psi^{\Delta}_{2m} + \phi_0^{\Delta}\psi^{\Sigma}_{2m}\right)\right], \end{aligned} \tag{3.18}$$

where $m = -2, 2, 0$. Since ψ^{Σ}_{2m} is a constant, without loss of generality, it can be set to zero and therefore terms $\psi^{\Sigma}_{2m}f^{2}_{2m}$ have been omitted in (3.17). The constant quantity

$$\Delta = \sum_{l,m} \tilde{a}(l) f_{lm} f^{*}_{lm} \tag{3.19}$$

defines the excess area as in the minimal model theories.

4. Results

The system of differential equations (3.17) and (3.18) is solved numerically using Matlab's ODE45 routine. For convenience, results for the real and complex components of the amplitudes are given,

$$f_{2m} = f'_{2m} + \mathrm{i}f''_{2m}, \quad \psi^{\Delta}_{2m} = \psi'^{\Delta}_{2m} + \mathrm{i}\psi''^{\Delta}_{2m}. \tag{4.1}$$

f'_{22}, f''_{22} and f_{20} specify deformations along the flow direction (x_1), the extensional axis ($x_1 = x_2$), and the vorticity direction (x_3). It should be noted that $f^{*}_{2m} = (-1)^m f_{2-m}$ and $\psi^{\Delta *}_{2m} = \psi^{\Delta}_{2-m}$ where $*$ denotes the complex conjugate. Vesicle orientation with respect to the flow direction is characterized by the inclination angle

$$\varphi_0 = -\frac{1}{2}\arctan\frac{f''_{22}}{f'_{22}}. \tag{4.2}$$

The numerical solutions of (3.17) and (3.18) reveal dynamics for the shape which is consistent with earlier theoretical work based on the minimal model (Misbah 2006; Vlahovska & Gracia 2007; Lebedev *et al.* 2008). Figure 2 illustrates vesicle shapes and time-dependent behaviour at various values of the viscosity ratio. Figure 3(*a*). shows the time dependence of each shape mode, and that at low viscosity ratio, $\eta = 1$, the vesicle shape and orientation approach a steady state with an inclination angle of $\varphi_0 \approx \pi/4$. This behaviour corresponds to the tank treading dynamics seen in the experimental work of Mader *et al.* (2006). In the final configuration, only the $f_{2\pm2}$ modes are nonzero which is also consistent with previous results (Vlahovska & Gracia 2007). At higher viscosity ratios, $\eta = 10$, the vesicle exhibits a tumbling motion characterized by a periodic oscillation in the shape modes, as illustrated in figure 3(b). In this leading order theory, the vacillating-breathing mode (Misbah 2006) is part of the tumbling solution and corresponds to time-dependent deformation along the

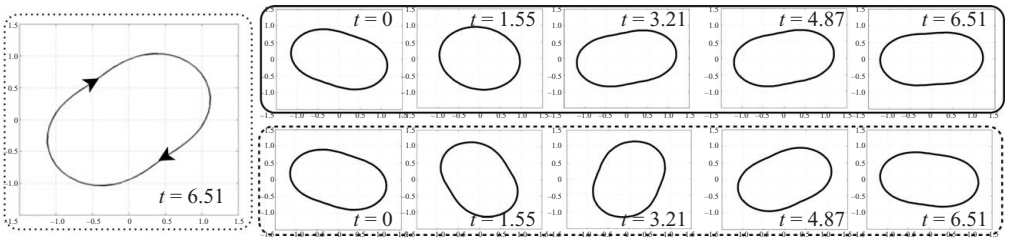

FIGURE 2. Contours of the vesicle shape as viewed from the vorticity axis for three different viscosity ratios. The image in the dotted box shows the long-time tank treading behaviour. The solid and dashed boxes show the vesicle behaviour at various times for the breathing ($\eta = 7$) and tumbling ($\eta = 100$) regimes, respectively. The times indicate when the snapshot was taken. All other parameters and initial conditions are the same as those in figure 3.

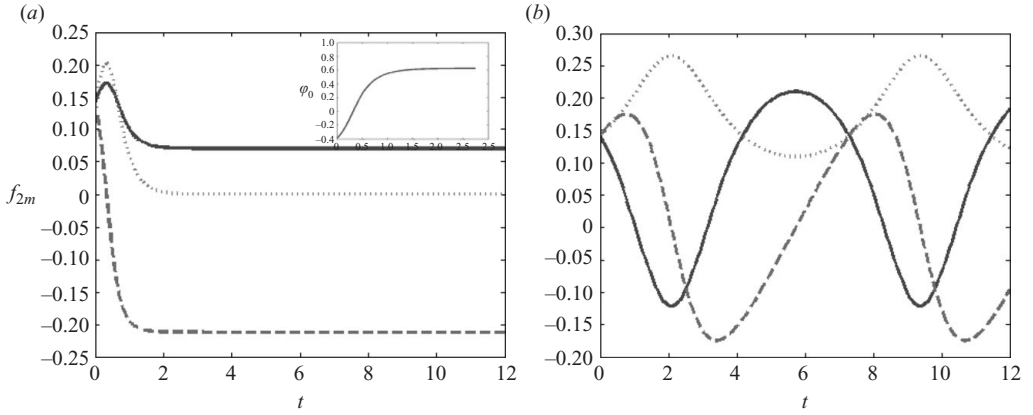

FIGURE 3. Time dependence of f_{2m} modes for (a) tank treading regime ($\eta = 1$) with the evolution of the inclination angle shown in the inset and (b) tumbling regime ($\eta = 10$). Both solutions are with $Ca = 1.0 \times 10^4$, $\beta = 1.33 \times 10^{10}$, $\Lambda = 1.33 \times 10^4$, $\alpha = 1.33 \times 10^8$ and $\phi_0^{\Delta} = 4 \times 10^{-4}$. The solid, dashed and dotted lines represent the f''_{22}, f'_{22} and f_{20} modes, respectively. The initial conditions for the $f_{2\pm2}$ are $f'_{22}(0) = f''_{22}(0) = \sqrt{0.1\Delta}$. The f_{20} mode is determined from(3.19) with $\Delta = 0.2$. Initial conditions for the density profiles are chosen as equilibrium configurations.

vorticity axis. In figure 3(b) the f_{20} mode is oscillating, which is a characteristic of the vacillating-breathing mode. Increasing the viscosity contrast damps this oscillation and in this case the vesicle executes pure tumbling motion.

Unlike earlier work, our theory gives insight into the dynamics of the lipids in the bilayer. Figure 4(a) shows that the lipids do indeed undergo an oscillatory (tank treading) motion even though the shape is constant. The density is oscillatory also in the tumbling regime, as seen in figures 4(b) and 4(c). Interestingly, at intermediate viscosity ratios $\eta = 10$, subharmonic oscillations are observed (see figure 4b), which disappear at high viscosity ratios. For $\eta = 1000$ the vesicle behaves as a tumbling rigid ellipsoid. Finally, the out-of-shear-plane mode ψ_{20}^{Δ} oscillates with an increasing amplitude as the viscosity increases from $\eta = 1$ to $\eta = 1000$.

Next we examine the effect of bilayer slip, which is equivalent to a difference in the fluid velocity on either side of the bilayer. Its reported values vary over a fairly wide range. Molecular dynamics simulations (den Otter & Shkulipa 2007) give b as $(2.4 - 7.3) \times 10^6$ Pa m^{-1}s which correspond to dimensionless β values of

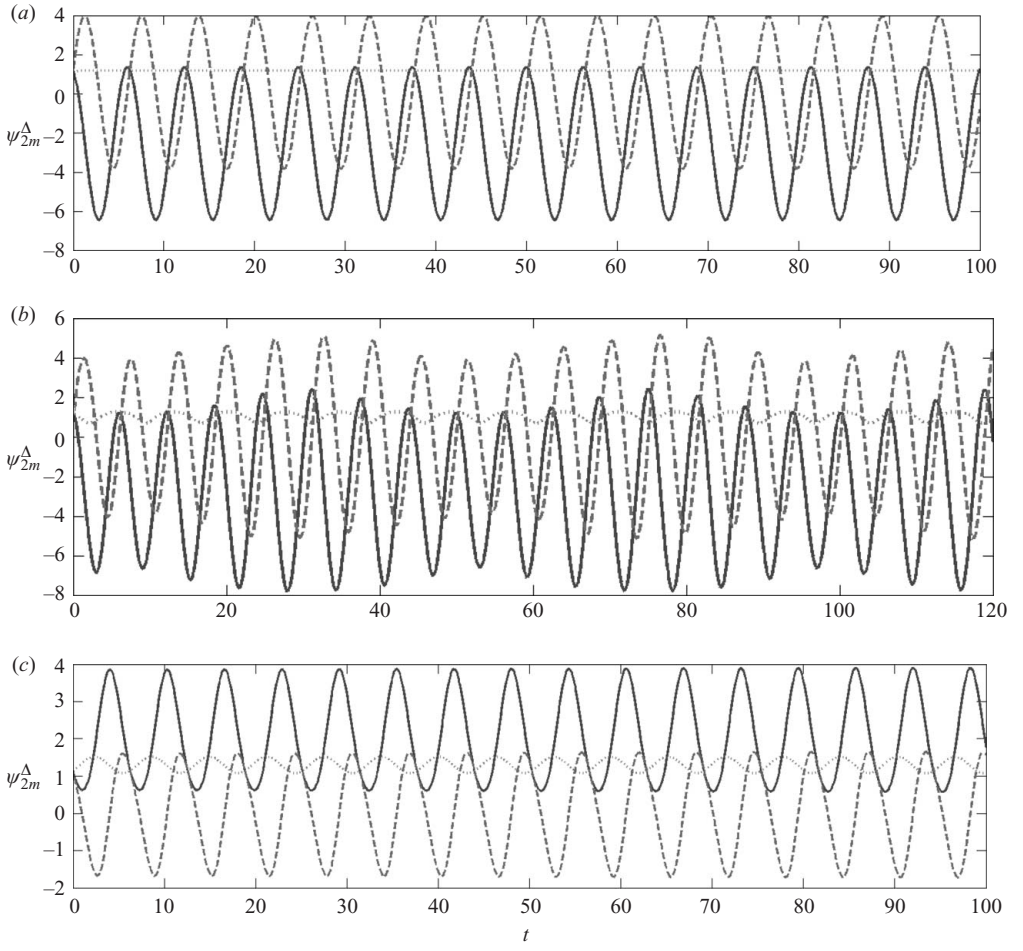

FIGURE 4. Time dependence of ψ_{2m}^{Δ} modes for viscosity ratios (*a*) $\eta = 1$, (*b*) $\eta = 10$ and (*c*) $\eta = 1000$. Other parameters are the same as in figure 3. The solid, dashed and dotted lines represent the $\psi_{22}^{\prime\prime\Delta}$, $\psi_{22}^{\prime\Delta}$ and ψ_{20}^{Δ} modes, respectively. All other parameters are the same as those in figure 2 and ψ_{2m}^{Δ} is rescaled by $\phi_0^{\Delta} = 4 \times 10^{-4}$.

$(0.13 - 0.39) \times 10^7$. Experimental measurements yielded β values $(1.6 - 160) \times 10^7$ (Merkel *et al.* 1989) or $(2.6 - 530) \times 10^8$ (Raphael & Waugh 1996). Figure 5 shows the long time dynamics of the density difference fields for two different values of the slip coefficient. In figure 5(*b*), for the lower value of β (1.33×10^4) one can see that the lipid density difference dynamics approach a constant value similar to that of shape modes in the tank treading regime. Small β means that the monolayers more easily slip past one another which may lead to more interesting dynamics. In figure 5(*a*) one can see a separation in the amplitudes of the $\psi_{22}^{\prime\prime\Delta}$ and $\psi_{22}^{\prime\Delta}$ modes as well as a secondary oscillation which occurs on a longer time scale. At high β, the monolayers move in tandem and the dynamics approaches the behaviour predicted by the minimal model.

In figure 6(*a*) the magnitude of the dimensionless slip velocity is shown for various values of β. One can see that as β decreases the magnitude of the velocity increases indicating that the monolayers can slide past one another with increasing ease. The

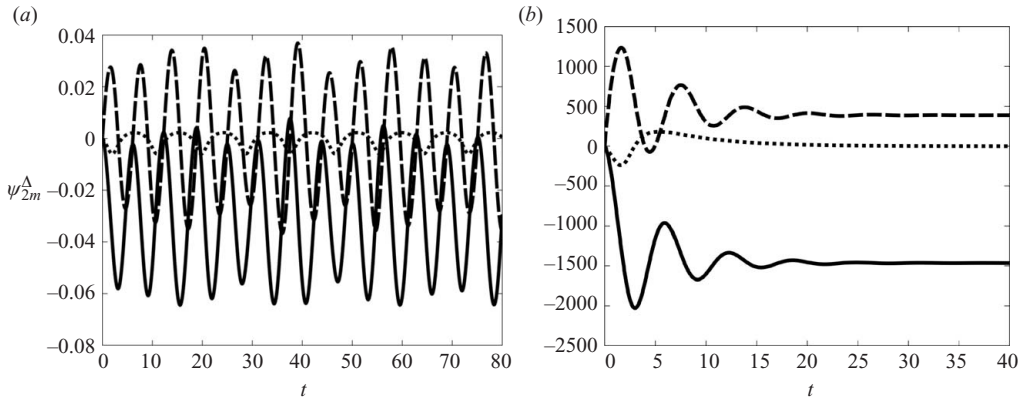

FIGURE 5. Time dependence of ψ_{2m}^{Δ} modes for (*a*) $\beta = 1.33 \times 10^8$ and (*b*) $\beta = 1.33 \times 10^4$ both solutions are with $\eta = 10$ and all other parameters the same as in figure 2. The solid, dashed and dotted lines represent the $\psi_{22}^{\prime\prime\Delta}$, $\psi_{22}^{\prime\Delta}$ and ψ_{20}^{Δ} modes, respectively, and ψ_{2m}^{Δ} is rescaled by $\phi_0^{\Delta} = 4 \times 10^{-4}$.

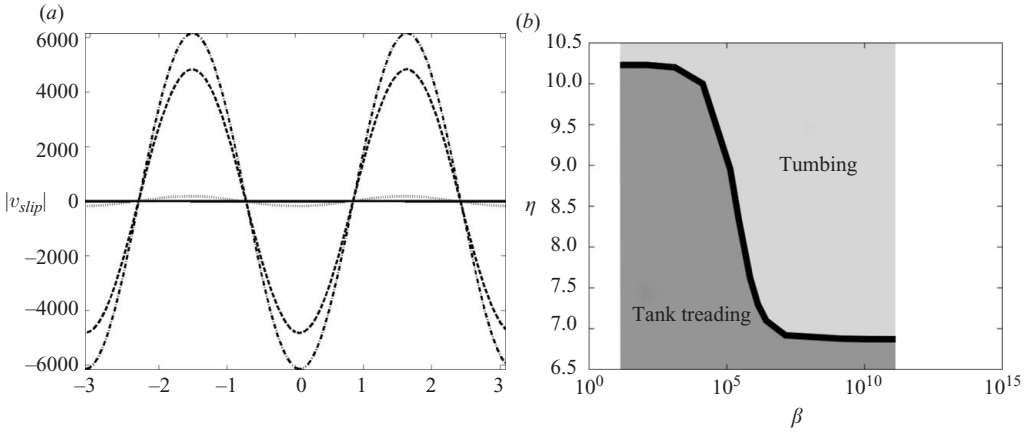

FIGURE 6. (*a*) The slip velocity as a function of angular position along the vesicle contour in the shear plane; the vesicle is in the tank treading regime ($\eta = 1$). The solid, dotted, dashed and dash-dotted lines correspond to β values of 10^{10}, 10^6, 10^4 and 10^2, respectively. All other parameters are the same as those in figure 3. (*b*) A phase diagram showing the critical viscosity contrast η_c, where the tank treading to tumbling bifurcation occurs for various values of β. All other parameters are the same as those in figure 3.

slip velocity is taken as positive if its component in the direction of the shearing flow is positive. Figure 6(*a*) implies that in some locations the slip velocity is pointed in the opposite direction of the shear flow.

The bilayer slip changes the critical viscosity contrast, η_c, where the tank-treading to tumbling transition occurs. A phase diagram for the parameters β and η is shown in figure 6 where the β axis is on a logarithmic scale. As the friction coefficient increases, the monolayer sheets encounter more resistance as they move relative to each other, and therefore behave as one entity. The plateau in figure 6(*b*) at large values of β shows a value of $\eta_c = 6.87$ which is close to that found by the minimal model theories (Misbah 2006; Vlahovska & Gracia 2007) for $\Delta \approx 0.2$ ($\eta_c = 7.16$). In addition to the variation in the critical viscosity, as β decreases from 10^{10} to 10^3

the period of oscillation in the shape modes increases from 7.28 to 11.3 units of dimensionless time, respectively. Smaller values of β were not examined because they are too far outside of the physical regime, where the Stokes' approximation is valid.

Finally it should be noted that equilibrium shapes and density profiles can be determined from (3.17) and (3.18) by setting the time derivatives on the left-hand side of the equations to zero and then solving the resulting system numerically for the unknowns. These solutions, and a linear analysis about these equilibrium solutions, can be shown to be consistent with the nonlinear dynamics found here as a function of η. For example, our numerical results show that in the tank treading regime ($\eta = 1$) equilibrium solutions can be found which correspond to the shapes predicted in figure 3(a), and the average value of the oscillatory density seen in figure 4(a), while in the tumbling regime ($\eta = 100$), the equilibrium solutions were found to be the average of the oscillations of both the shape and density modes.

5. Conclusions

This study considers the dynamics of a vesicle formed by a fluid phospholipid bilayer membrane in a viscous flow. We have adopted a general model for the membrane which accounts for the bilayer architecture and allows the two constituent monolayers to slide past one another. In addition to this, bilayer bending resistance, monolayer compressibility, viscosity of the surrounding fluids and the fixed number of lipid molecules per monolayer are taken into account. The limit of a nearly spherical vesicle is examined and analytical results are obtained for the shape and density evolution, velocity fields and effective isotropic membrane tension. The resulting evolution equations (3.17) and (3.18) are nonlinear.

Numerical integration of the evolution equations yielded similar dynamics for the shape as seen in earlier work based on the minimal model (Misbah 2006; Vlahovska & Gracia 2007), namely a transition from a tank treading state to a tumbling state. Our work allows for a first time to examine two phenomena: firstly, the evolution of the lipid density fields on the monolayers, and secondly, the slipping of the monolayers relative to one another. Novel features are observed, e.g. as the viscosity ratio increases, subharmonic oscillations appear in the evolution of the density fields which damp out as the $\eta \to \infty$. The bilayer slip is an additional parameter which modifies the critical viscosity where the tank treading to tumbling transition occurs.

Equations (3.12) and (3.13) are valid for external flow fields for arbitrary geometry and therefore can be used to describe the dynamics of a lipid bilayer vesicle in Poiseuille flow. This work can be used as a foundation to study other phenomena which require knowledge of the density fields such as pore formation.

This paper is dedicated to Professor Stephen H. Davis on the occasion of his 70th birthday. J. T. S. and M. J. M. were supported in part by NSF RTG grant no. DMS-0636574 and NSF grant no. DMS-0616468. P. M. V. acknowledges financial support by NSF CAREER award CBET-0846247.

Appendix A. Stress balance

The inner and outer components of the tangential forces in (2.5) can be summed to give

$$\left(\boldsymbol{t}^{+}_{rs,t} + \boldsymbol{t}^{-}_{rs,t}\right) + \left(\boldsymbol{t}^{+}_{hd,t} + \boldsymbol{t}^{-}_{hd,t}\right) = 0, \tag{A 1}$$

and subtracted to give

$$\left(\boldsymbol{t}^{+}_{rs,t}-\boldsymbol{t}^{-}_{rs,t}\right)+\left(\boldsymbol{t}^{+}_{hd,t}-\boldsymbol{t}^{-}_{hd,t}\right)-2b\left(\boldsymbol{v}^{+}_{s}-\boldsymbol{v}^{-}_{s}\right)=0. \tag{A 2}$$

The jump in the normal stress is balanced by the membrane forces,

$$\left(\boldsymbol{t}^{+}_{rs}+\boldsymbol{t}^{-}_{rs}\right)\cdot\boldsymbol{n}+\left(\boldsymbol{t}^{+}_{hd}+\boldsymbol{t}^{-}_{hd}\right)\cdot\boldsymbol{n}=0. \tag{A 3}$$

A.1. *Linearization of membrane forces*

For small perturbations from sphericity, the mean and Gaussian curvatures can be expressed as sums of scalar spherical harmonics, $H=-1-1/2\sum_{l,m}(l+2)(l-1)f_{lm}\mathscr{Y}_{lm}$, and $K=1+\sum_{l,m}(l+2)(l-1)f_{lm}\mathscr{Y}_{lm}$. Note that here and below we suppress the linearization parameter ϵ from the equations. The surface gradient operator is evaluated on a sphere,

$$\nabla_s=\boldsymbol{e}_\theta\frac{\partial}{\partial\theta}+\boldsymbol{e}_\phi\frac{1}{\sin\theta}\frac{\partial}{\partial\phi}, \tag{A 4}$$

and the Laplace–Beltrami operator becomes $\Delta=\nabla_s\cdot\nabla_s=-\widehat{L}^2$ which at leading order is the angular component of the Laplacian in spherical coordinates,

$$-\widehat{L}^2=\frac{1}{\sin\theta}\frac{\partial}{\partial\theta}\left(\sin\theta\frac{\partial}{\partial\theta}\right)+\frac{1}{\sin^2\theta}\frac{\partial^2}{\partial\phi^2}. \tag{A 5}$$

The spherical harmonics satisfy the eigenvalue relationship, $\widehat{L}^2\mathscr{Y}_{lm}=l(l+1)\mathscr{Y}_{lm}$.

Insertion of these expressions in (2.6), gives the leading order normal component of the membrane elastic force,

$$\left(\boldsymbol{t}^{+}_{rs}+\boldsymbol{t}^{-}_{rs}\right)\cdot\boldsymbol{e}_{\boldsymbol{r}}=-2\widetilde{\tau}-\sum_{l,m}\left[E_l f_{lm}-4\alpha\psi^{\Sigma}_{lm}-\left[4\alpha\phi^{\Delta}_0+\Lambda(l+2)(l-1)\right]\psi^{\Delta}_{lm}-2\sigma_{lm}\right]\mathscr{Y}_{lm}, \tag{A 6}$$

where $E_l=(l+2)(l-1)\left[l(l+1)+\frac{\tau_0}{\mathscr{S}}\right]$, $\tau_0=\widetilde{\tau}+\Lambda\phi^{\Delta}_0$ and lastly, $\widetilde{\tau}=\sigma_0+\Lambda\phi^{\Delta}_0-\alpha(\phi^{\Delta}_0)^2$.

In place of the θ and ϕ components of the tangential traction, it is more convenient to use the surface divergence and surface curl. Taking divergence of (A 1) and (A 2) leads to

$$\nabla_s\cdot\left(\boldsymbol{t}^{+}_{rs,t}-\boldsymbol{t}^{-}_{rs,t}\right)=\sum_{l,m}l(l+1)\left[2\alpha\psi^{\Delta}_{lm}-\Lambda(l+2)(l-1)f_{lm}+2\alpha\phi^{\Delta}_0\psi^{\Sigma}_{lm}\right]\mathscr{Y}_{lm}, \tag{A 7}$$

$$\nabla_s\cdot\left(\boldsymbol{t}^{+}_{rs,t}+\boldsymbol{t}^{-}_{rs,t}\right)=\sum_{l,m}l(l+1)\left[\sigma_{lm}+2\alpha\psi^{\Sigma}_{lm}-\Lambda\phi^{\Delta}_0(l+2)(l-1)f_{lm}+2\alpha\phi^{\Delta}_0\psi^{\Delta}_{lm}\right]\mathscr{Y}_{lm}. \tag{A 8}$$

The surface curl component is identically zero.

A.2. *Bulk hydrodynamics*

Here we list the hydrodynamic tractions corresponding to the classical Lamb solution to the Stokes' equations around a sphere. More details can be found in Seifert (1999). The interior velocity is expressed as an infinite sum of growing harmonics

$$\boldsymbol{v}^{in}(r)=\sum_{l\geqslant 2}\left(\nabla\sum_{m=-l}^{l}\left(\Phi^{in}_{lm}\mathscr{Y}_{lm}r^l\right)+M(l)r^2\nabla\sum_{m=-l}^{l}\left(p^{in}_{lm}\mathscr{Y}_{lm}r^l\right)-N(l)\boldsymbol{r}\sum_{m=-l}^{l}\left(p^{in}_{lm}\mathscr{Y}_{lm}r^l\right)\right). \tag{A 9}$$

The expansion coefficients, Φ^{in}_{lm} and p^{in}_{lm} are linear combinations of scalar fields $X^{(a)}=\boldsymbol{v}^{\pm}\cdot\boldsymbol{e}_r$, $Y^{(a)}=-\nabla_s\cdot\boldsymbol{v}^{\pm}$ and $Z^{(a)}=\boldsymbol{e}_r\cdot(\nabla_s\times\boldsymbol{v}^{\pm})$ where each of these is expanded

in scalar harmonics $X_{lm}^{(a)}$, $Y_{lm}^{(a)}$ and $Z_{lm}^{(a)}$, respectively. The quantities $M(l)$ and $N(l)$ are rational functions of the harmonic mode l and given in Happel & Brenner (1983) as

$$M(l) = \frac{l+3}{2\eta(l+1)(2l+3)}, \quad N(l) = \frac{l}{\eta(l+1)(2l+3)}. \tag{A 10}$$

The exterior velocity field is obtained by making the substitution, $l \to -l-1$, which leads to a sum of harmonics decaying with distance, and making $\eta = 1$.

The extensional component of the imposed shear flow is linear with the distance and therefore it is specified by growing harmonics of order $l = 2$ and amplitudes $X_{2\pm2}^{\infty} = Y_{2\pm2}^{\infty} = \mp \mathrm{i}\sqrt{2\pi/15}$.

The normal component of the hydrodynamic tractions is

$$\boldsymbol{t}_{hd,r}^{out} = -\sum_{l,m} \left[a_l^{out} X_{lm}^{out} + b_l^{out} Y_{lm}^{out} + a_l^{in} X_{lm}^{\infty} + b_l^{in} Y_{lm}^{\infty}\right] \mathscr{Y}_{lm}, \tag{A 11}$$

$$\boldsymbol{t}_{hd,r}^{in} = -\sum_{l,m} \left[a_l^{in} X_{lm}^{in} + b_l^{in} Y_{lm}^{in}\right] \mathscr{Y}_{lm}. \tag{A 12}$$

The components tangential to a sphere, once an extra surface gradient is taken are,

$$\boldsymbol{t}_{hd,t}^{out} = \sum_{l,m} \left[c_l^{out} X_{lm}^{out} + d_l^{out} Y_{lm}^{out} + c_l^{in} X_{lm}^{\infty} + d_l^{in} Y_{lm}^{\infty}\right] \mathscr{Y}_{lm}, \tag{A 13}$$

$$\boldsymbol{t}_{hd,t}^{in} = \sum_{l,m} \left[c_l^{in} X_{lm}^{in} + d_l^{in} Y_{lm}^{in}\right] \mathscr{Y}_{lm}. \tag{A 14}$$

Since a rotational type flow Z_{lm} can not be excited by elastic membrane stresses (recall that the surface curl of the membrane tractions vanishes), the second tangential component of the tractions is not relevant to this study. In shear flow, it is automatically satisfied by rigid body rotation. Expressions for the l-dependent coefficients in equations (A 11)–(A 14) can be found in Miao *et al.* (2002).

Appendix B. Evolution equations for shape and lipids

The kinematic equations and the continuity of lipids equations existing on both monolayer surfaces provide the link between the Lamb velocity, $X_{lm}^{(a)}$ and $Y_{lm}^{(a)}$, and the amplitudes of the perturbation fields. To leading order in ϵ, (2.4) reads as,

$$\nabla_s \cdot \boldsymbol{v}_s^{\pm} = -\frac{\mathrm{d}\phi^{\pm}}{\mathrm{d}t} - 2\frac{\mathrm{d}f_{lm}}{\mathrm{d}t}. \tag{B 1}$$

Kinematic matching of the surface velocity to the adjacent bulk fluid yields, to order ϵ, the evolution equation for the shape

$$\frac{\mathrm{d}f_{lm}}{\mathrm{d}t} = X_{lm}^{out} = X_{lm}^{in} \tag{B 2}$$

and the lipid densities

$$\frac{\mathrm{d}\psi_{lm}^{+}}{\mathrm{d}t} = Y_{lm}^{out}, \quad \frac{\mathrm{d}\psi_{lm}^{-}}{\mathrm{d}t} = Y_{lm}^{in}, \tag{B 3}$$

where X_{lm} are amplitudes of the radial Lamb velocity field and Y_{lm} are amplitudes of the velocity field tangential to a sphere.

Appendix C. Coefficients and membrane tension

After some tedious algebra, we derive the coefficients in (3.12)

$$\Gamma(\eta, l) = -(1+\eta)(2l^3+3l^2) - 4\eta + 5, \tag{C 1}$$

$$a(l) = (l+2)(l-1), \tag{C 2}$$

$$J(\eta, l) = \left[(2+l)(1-\eta) - 3\right], \tag{C 3}$$

$$C(l, \pm l) = \pm l(l+1)\left[\left(2c_l^{in} - a_l^{in}\right)X_{lm}^{\infty} + \left(2d_l^{in} - b_l^{in}\right)Y_{lm}^{\infty}\right], \tag{C 4}$$

$$D(l) = \Lambda l(l+1)a(l). \tag{C 5}$$

The coefficients in (3.13) are

$$\hat{\Gamma}(\eta, l) = (\eta-1)l + 2\eta + 1, \tag{C 6}$$

$$\hat{C}(l, \pm l) = \pm l(l+1)\left(c_l^{in}X_{lm}^{\infty} + d_l^{in}Y_{lm}^{\infty}\right), \tag{C 7}$$

$$\hat{J}(\eta, l) = (2l+1)(1+\eta) + 2\chi^{-1}\beta. \tag{C 8}$$

The isotropic tension σ_0 is obtained from (3.11) in conjunction with equations (3.12) and (3.13). Equation (3.12) is solved for $\dot{f}_{lm}$ and the result is multiplied by $\tilde{a}(l)f_{lm}^*$. Summing over all modes and enforcing (3.11) leads to an equation for σ_0 which yields

$$\sigma_0 = -\frac{\sum_{l,m}\Gamma^{-1}\tilde{a}(l)\left[-Jf_{lm}^*\dot{\psi}_{lm}^{\Delta} + Cf_{lm}^* + \chi^{-1}l(l+1)\tilde{E}_l f_{lm}f_{lm}^* - \chi^{-1}Df_{lm}^*\psi_{lm}^{\Delta}\right]}{\chi^{-1}\sum_{l,m}\Gamma^{-1}l(l+1)\tilde{a}(l)a(l)f_{lm}f_{lm}^*}. \tag{C 9}$$

Thus the isotropic tension couples all modes. Inserting the above expression in (3.12) leads to the nonlinear shape evolution (3.17).

REFERENCES

Abkarian, M. & Viallat, A. 2008 Vesicles and red blood cells in shear flow. *Soft Matter* **4**, 653–657.

Alberts, B. 2002 *Molecular Biology of the Cell*. Garland Science.

Allen, T. M. & Cullis, P. R. 2004 Drug delivery systems: entering the mainstream. *Science* **303**, 1818–1822.

Aris, R. 1989 *Vectors, Tensors, and the Basic Equations of Fluid Mechanics*. Dover.

Barthes-Biesel, D. 1991 Role of interfacial properties on the motion and deformation of capsuled in shear flow. *Physica* A **172**, 103–124.

Barthes-Biesel, B. & Rallison, J. 1981 The time-dependent deformation of a capsuel freely suspended in a linear shear flow. *J. Fluid Mech.* **113**, 251–267.

Brown, F. L. 2008 Elastic modeling of biomembranes and lipid bilayers. *Annu. Rev. Phys. Chem.* **59**, 685–712.

Cai, W. & Lubensky, T. 1995 Hydrodynamics and dynamic fluctuations of fluid membranes. *Phys. Rev.* E **52** (4).

Danker, G., Biben, T., Podgorski, T., Verdier, C. & Misbah, C. 2007 Dynamics and rheology of a dilute suspension of vesicles: higher order theory. *Phys. Rev.* E **76**, 041905.

Danker, G., Vlahovska, P. M. & Misbah, C. 2009 Vesicles in Poiseuille flow. *Phys. Rev. Lett.* **102**, 148102.

Deschamps, J., Kantsler, V. & Steinberg, V. 2009 Phase diagram of single vesicle dynamical states in shear flow. *Phys. Rev. Lett.* **102**, 118105.

Dimova, R., Aranda, S., Bezlyepkina, N., Nikolov, V., Riske, K. A. & Lipowsky, R. 2006 A practical guide to giant vesicles. Probing the membrane nanoregime via optical microscopy. *J. Phys.: Condens. Matter* **18**, S1151–S1176.

Dobereiner, H.-G., Evans, E., Kraus, M., Seifert, U. & Wortis, M. 1997 Mapping vesicle shapes into phase drigram: a comparison of experiment and theory. *Phys. Rev.* E **55** (4), 4458–4474.

Edwards, D. A., Brenner, H. & Wasan, D. T. 1991 *Interfacial Transport Processes and Rheology*. Butterworth-Heinemann.

Evans, E., Yeung, A., Waugh, R. & Song, J. 1992 Dynamic coupling and nonlocal curvature elasticity in bilayer membranes. In *The Structure and Conformation of Amphiphilic Membranes*, vol. 66, (ed. R. Lipowsky, D. Richter & K. Kremer) pp. 148–153. Springer Proceedings in Physics.

Goldstein, R., Nelson, P., Powers, T. & Seifert, U. 1996 Front propogation in the pearling instability of tubular vesicles. *J. Phys.* II *France* **6**, 767–796.

Happel, J. & Brenner, H. 1983 *Low Reynolds Number Hydrodynamics*. Martinus Nijhoff.

Helfrich, W. 1973 Elastic properties of lipid bilayers. *Z. Naturforsch* **28c**, 693–703.

Jenkins, J. T. 1977 Static equilibrium configurations of a model red blood cell. *J. Math. Biol.* **4**, 149–169.

Kantsler, V. & Steinberg, V. 2005 Orientation and dynamics of a vesicle in tank-treading motion in shear flow. *Phys. Rev. Lett.* **95**.

Kantsler, V. & Steinberg, V. 2006 Transition to toumbling and two regimes of toumbling motion of a vesicle in shear flow. *Phys. Rev. Lett.* **96**.

Lebedev, V. V., Turitsyn, K. & Vergeles, S. S. 2008 Nearly spherical vesicles in an external flow. *New J. Phys.* **10** (043044).

Lipowsky, R. 1991 The conformation of membranes. *Nature* **349**, 475–481.

Mader, M.-A., Vitkova, V., Abkarian, M., Viallat, A. & Podgorski, T. 2006 Dynamics of viscous vesicles in shear flow. *Eur. Phys. J.* E **19**, 389–397.

Merkel, R., Sackmann, E. & Evans, E. 1989 Molecular friction and epitactic coupling between monolayers in supported bilayers. *J. Phys. France* **50**, 1535–1555.

Miao, L., Lomholt, M. & Kleis, J. 2002 Dynamics of shape fluctuations of quasi-spherical vesicles revisited. *Eur. Phys. J.* E **9**, 143–160.

Milner, S. & Safran, S. 1987 Dynamical fluctuations of droplet microemulsions and vesicles. *Phys. Rev.* A **36** (9), 4371–4379.

Misbah, C. 2006 Vacillating breathing and tumbling of vesicles under shear flow. *Physical Rev. Lett.* **96**, 028104.

Morse, P. & Feshbach, H. 1953 *Methods of Theoritical Physics*. McGraw-Hill.

Olla, P. 2000 The behavior of closed inextensible membranes in linear and quadratic shear flows. *Physica* A **278**, 87–106.

den Otter, W. & Shkulipa, S. 2007 Intermonolayer friction and surface shear viscosity of lipid bilayer membranes. *Biophys. J.* **93**, 423–433.

Pozrikidis, C. 2003 *Modeling and Simmulation of Capsules and Biological Cells*. CRC Press.

Raphael, R. & Waugh, R. 1996 Accelerated interleaflet transport of phosphatidylcholine molecules in membranes under deformation. *Biophys. J.* **71**, 1374–1388.

Schneider, M., Jenkins, J. & Webb, W. 1984 Thermal fluctuations of large quasi-spherical biomolecular phospholipid vesicles. *J. Phys.* **45**, 1457–1472.

Seifert, U. 1997 Configurations of fluid membranes and vesicles. *Adv. Phys.* **46** (1), 13–137.

Seifert, U. 1999 Fluid membranes in hydrodynamic flow fields: formalism and an application to fluctuating quasispherical vesicles in shear flow. *Eur. Phys. J.* B **8**, 405–415.

Seifert, U., Berndl, K. & Lipowsky, R. 1991 Shape transformation of vesicles: phase diagram for spontaneous-curvature and bilayer-coupling models. *Phys. Rev.* A **44** (2), 1182–1202.

Seifert, U. & Langer, S. 1993 Viscous modes of fluid bilayer membranes. *Europhys. Lett.* **23** (1), 71–76.

Stone, H. 1990 A simple derivation of the time-dependent convective-diffusion equation for surfactant transport along a deforming interface. *Phys. Fluids* A **2** (1), 111–112.

Vlahovska, P. & Gracia, R. 2007 Dynamics of a viscous vesicle in linear flows. *Phys. Rev.* E **75** (016313).

Yeung, A. & Evans, E. 1995 Unexpected dynamics in shape fluctuations of bilayer vesicles. *J. Phys.* II *France* **5**, 1501–1523.